Journal of Power Sources 184 (2008) 229–237

Contents lists available at ScienceDirect

Journal of Power Sources

journal homepage: www.elsevier.com/locate/jpowsour

Fabrication of an anode-supported yttria-stabilized zirconia thin film for solid-oxide fuel cells via wet powder spraying

Wei Zhou, Huangang Shi, Ran Ran, Rui Cai, Zongping Shao*, Wanqin Jin

State Key Laboratory of Materials-Oriented Chemical Engineering, College of Chemistry & Chemical Engineering, Nanjing University of Technology, No. 5 Xin Mofan Road, Nanjing 210009, PR China

ARTICLE INFO

Article history:
Received 9 May 2008
Received in revised form 1 June 2008
Accepted 4 June 2008
Available online 20 June 2008

Keywords:
Solid-oxide fuel cells (SOFCs)
Thin electrolyte film
Yttria-stabilized zirconia (YSZ)
Wet powder spraying (WPS)

ABSTRACT

The wet powder spraying (WPS) technique was used for the deposition of dense and thin $(Y_2O_3)_{0.08}(ZrO_2)_{0.92}$ (YSZ-8) films on an anode substrate being used for fuel cell applications. Both agglomeration of the powder and the presence of organics in the substrate have a significant effect on the quality and densification of the thin electrolyte layer. High-energy ball milling effectively broke up the agglomerates and enhanced the packing density of the green layer. Pre-calcination of the substrate at ~1000 °C enhanced the match of sintering shrinkage between the electrolyte layer and the substrate and improved the quality of the YSZ-8 thin film significantly. Crack-free dual-layer assembly with a highly densified YSZ-8 film as thin as 10 μm was successfully fabricated by optimizing the fabrication parameters. The cells with a $La_{0.8}Sr_{0.2}MnO_3$ cathode showed a high open circuit voltage of 1.071 V and a peak power density of 894 mW cm^{-2} at 850 °C operated with hydrogen fuel.

1. Introduction

Yttria-stabilized zirconia (YSZ) membranes are the most widely applied solid-state electrolytes of high-temperature oxygen sensors, solid-oxide fuel cells (SOFCs), and electrolyzers, because of their high ionic conductivity at elevated temperatures, good thermal/chemical stability, and favorable mechanical strength. For SOFCs based on a thick YSZ electrolyte, an operating temperature as high as 1000 °C is necessary to achieve high power density, which, however, puts stringent requirement on the sealing and also induces a rapid degradation of cell performance due to the high solid-state reaction rate between cell components. In order to solve or avoid the above problems, extensive research has been conducted to reduce the operating temperature of SOFCs to an intermediate range of 500–800 °C. However, since the ionic conductivity of YSZ decreases obviously with the drop in temperature, the development of new electrolyte materials with improved ionic conductivities at reduced temperature has been proposed to ensure a high power density at intermediate temperature [1–3]. A reduction of the electrolytic thickness has also been proposed [4].

A number of coating techniques such as chemical vapor deposition (CVD), physical vapor deposition (PVD), electrochemical vapor deposition (EVD), and ceramic powder processes have been exploited to fabricate dense YSZ electrolyte on porous substrates for SOFC applications [5–20]. Among these techniques, ceramic powder processes [11–14] such as tape casting [15,16], slurry coating [17,18], and screen-printing [19,20] are economical and efficient techniques for ceramic coating; however, they are only appropriate for flat cells. Furthermore, the large shrinkage associated with the removal of polymeric binders and plasticizers in subsequent sintering steps may reduce the quality of large area cells.

Wet powder spraying (WPS) has been successfully used as a processing technique for forming porous gas electrodes [21–24]. This process does not require as much binder as the ceramic powder processes. More importantly, WPS is a non-contact technique that is highly suitable for engineering structures, for example, functionally graded electrodes. Furthermore, it is also applicable to a variety of surfaces, corrugated sheets, and tubes. Compared to most of the above-mentioned deposition techniques, the deposition rates of WPS are high and the fabrication costs are low. Moreover, it has a high potential for up-scaling from laboratory to industrial fabrication. Schüller et al. [25] demonstrated that the WPS process is a practicable method to produce a thin gas-tight electrolyte layer by optimizing the suspensions in solid content and viscosity. Recently, this method has been successfully applied to prepare thin electrolyte film for SOFCs [26,27]. However, there are few studies concerning the preparation process of this technique. In this paper, we present detailed investigation of the WPS process for the fabrication of an anode-supported YSZ thin film for SOFC application. Attention was paid to the effects of powder agglomeration and

* Corresponding author. Tel.: +86 25 83587722; fax: +86 25 83365813.
E-mail address: shaozp@njut.edu.cn (Z. Shao).

0378-7753/$ – see front matter © 2008 Elsevier B.V. All rights reserved.
doi:10.1016/j.jpowsour.2008.06.021

the properties of the anode substrate on thin film formation and densification.

2. Experimental

2.1. Preparation of powder and anode-support

All the raw materials applied in this study were provided from Sinopharm Chemical Reagent Co. Ltd., Shanghai, China in analytical grade. $(Y_2O_3)_{0.08}(ZrO_2)_{0.92}$ (YSZ-8) powders were synthesized using a combined EDTA–citrate complexing sol–gel process with the detailed procedure referred to our previous publication [28]. $Y(NO_3)_3{\cdot}6H_2O$ and $Zr(NO_3)_4{\cdot}5H_2O$ were prepared in a mixed solution followed by the addition of EDTA and citric acid in sequence at a pH value of ~6 with the help of NH_4OH with a mole ratio of total metal ions:EDTA:citric acid of 1:1:2. Evaporating the water at 90 °C resulted in the transparent gels, which were then pre-fired at 250 °C and further calcined at 900 °C for 5 h in air to give the final products.

The anode substrate was prepared by a dry-pressing method. A mixture consisting of well-mixed 57 wt.% NiO, 38 wt.% YSZ, and 5 wt.% PVB was dropped into a stainless steel die with a diameter of 15 mm and then pressed under 200 MPa for 1 min. The green pellets were directly applied as the substrates for spray deposition of the thin electrolyte film, or they were pre-calcined before deposition at 900–1400 °C for 5 h to get rid of the organics within the substrates and to modify their shrinkage.

2.2. Preparation of suspension

The suspension for spray deposition was prepared as follows. About 2 g of the YSZ-8 powder and 20 g of ethylene glycol (EG) were mixed with 60 g of zirconia grinding media in an 80 mL zirconia container and agitated on a high-energy miller (Model Pulverisette 6, Fritsch, Germany) with a rotational speed of 500 rpm for 30 min. After the milling, additional ethylene glycol was added to the YSZ suspension to reach a total ethylene glycol amount of 80 g. No further additives such as binders, plasticizers, or dispersants were used. The powder content in the diluted suspension was around 2.4 wt.%. For a comparative study, an YSZ-8 powder suspension was also prepared by mixing 1 g of the YSZ-8 powders and 40 g of the ethylene glycol in an agate mortar for 30 min with the help of manual grinding.

2.3. WPS process and fabrication of single cell

The suspension was sprayed onto the anode substrate using a modified spraying gun (BD-128, Fenghua Bida Machinery Manufacture Co. Ltd., Fenghua, China) with a nozzle size of 0.35 mm (diameter). Nitrogen was used as the carrier gas at a working pressure of 1 atm. The spraying gun was aligned vertically to the anode substrate leaving a 10 mm distance between them. The spray speed was controlled at about 0.005 g (YSZ-8) s^{-1}. The spray process was carried out at a substrate temperature of ~200 °C with the help of a hot plate. After the spray deposition, the green dual-layer pellets were fired at 1400 °C in air for 5 h at a heating rate of 3 °C min^{-1}. $La_{0.8}Sr_{0.2}MnO_3$ (LSM) slurry was then painted on the central surface of the electrolyte by brush and fired at 1150 °C for 5 h in air to function as the cathode layer. The resulting coin-shape cathode had a thickness of ~20 μm and an effective area of 0.5 cm^2.

2.4. Characterization

Crystal structures of the synthesized powders were determined by X-ray diffraction (XRD; Model D8 Advance, Bruker, Germany) using Cu Kα radiation (λ = 1.5418 Å). The crystallite domain sizes (D) were examined from XRD peaks based on the Scherrer equation, $D = 0.9\lambda/(B\cos\theta)$, where λ is the X-ray wavelength, θ is the Bragg diffraction angle, and B is the calibrated half-peak width of the XRD lines. The experimental diffraction patterns were collected at room temperature by step scanning in the range of $20^\circ \le 2\theta \le 80^\circ$.

The particle size distribution of the milled powders was measured with a particle size analyzer (Zetasizer 3000, Malvern Instruments, Malvern, UK). The particle size and the morphology of the derived YSZ-8 powders were also examined with a transmission electron microscope (TEM; Tecnai G20, FEI. Co. Ltd., Eindhoven, Netherlands) and a field emission scanning electron microscope (FESEM; Sirion 200, FEI. Co. Ltd., Philips, Netherlands). The morphology of the YSZ-8 film was observed using an environmental scanning electron microscope (ESEM; Model QUANTA-2000, FEI Company, Hillsboro, OR).

Packing density of the green YSZ-8 thin film on the anode-substrate was estimated by assuming it was identical to the green density of the corresponding electrolyte powders. In some cases, it was also estimated from the volume change of the thin film before and after sintering by measuring the diameter of the anode substrate with a vernier caliper and the thin-film thickness using SEM and assuming that the relative density of the thin-film layer is 100% after the sintering.

An in-house constructed fuel cell test station was applied for electrochemical performance evaluation of the fabricated cells. Humidified (3% H_2O) H_2 at a flow rate of 80 mL min^{-1} [STP] was fed into the anode as fuel and air 400 mL min^{-1} [STP] was used as the cathode atmosphere. I–V polarization curves were collected at intervals of 50 °C over a temperature range of 850–700 °C using a digital electrometer (Model 2420, Keithley, Cleveland, OH) based on a four-probe configuration. Mass flow controllers were used to control flow rates. Silver paste (DAD-87, Shanghai Institute of Synthesized Risen) was painted on the outer surface of the cathode and then fired at 250 °C to get rid of organics as a current collector. Electrochemical impedance spectra (EIS) of the single cells were measured by Solartron-1260 frequency responding analyzer combined with Solartron-1287 electrochemical interface. The EIS were recorded in a frequency range of 10 kHz to 1 Hz with signal amplitude of 30 mV under open circuit voltage (OCV).

3. Results and discussion

Fig. 1 shows the XRD pattern of the as-prepared YSZ-8 powders after they were calcined at various temperatures in air for 5 h. At a temperature of >500 °C, a crystallized phase was formed. All the diffraction peaks can be well indexed to a cubic fluorite lattice structure, implying the successful formation of pure phase fluorite oxide. The crystallite size calculated based on the Scherrer equation for the powder calcined at 900 °C is about 22.1 nm. The particle distribution of the YSZ suspension after the manual grinding is shown in Fig. 2. It shows two distribution zones with an average particle sizes of 210 (36.1 vol%) and 1170 nm (63.9 vol%), respectively. Both particle sizes are much larger than the crystallite size, suggesting that the agglomeration formed in the YSZ-8 powders prepared from the EDTA–citrate combined complexing process even after the manual grinding. The powder was further investigated by FESEM and TEM observations with the results shown in Fig. 3. It clearly shows that the powder was mainly composed of small primary particles with a grain size of ~200 nm, which was highly densified and free of pores or voids (Fig. 3a), suggesting the sintering of the primary particles. Such particles agglomerated seriously to form larger particles containing many voids and pores, as shown in Fig. 3b and c.

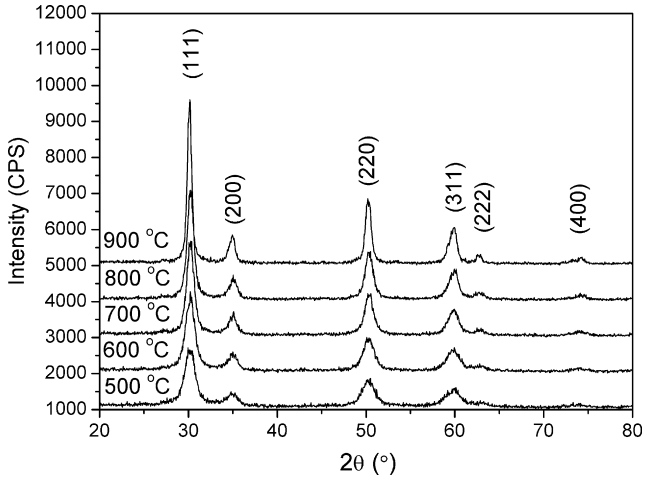

Fig. 1. XRD patterns of the YSZ-8 powders calcined at various temperatures.

The surface morphology of the sintered YSZ-8 electrolyte with the 900 °C calcined powder ground manually is shown in Fig. 4a. Many cracks were observed over the membrane surface after the sintering at 1400 °C for 5 h. For the dual-layer membrane, the shrinking and densification behaviors of each layer were affected by the other layer during the sintering. Considering that the anode-substrate (500–1000 μm) is much thicker than the electrolyte (10–50 μm), the sintering behavior of the thin electrolyte film was influenced more significantly by the anode than the anode by the thin film. In order to get a crack-free and fully densified YSZ-8 thin film, the shrinkage of the anode-substrate and the thin electrolyte film should be tailored. Under the most ideal situation, the shrinkage of the anode-substrate (S_A) should be equal to that of the thin electrolyte film (S_E) required for a fully densified electrolyte

$$S_A = S_E. \quad (1)$$

Assuming that the shrinkage of the YSZ thin film is identical in all three dimensions, it can be expressed by

$$S_E = \frac{D_0 - D_1}{D_0} = \frac{d_0 - d_1}{d_0} = 1 - \frac{D_1}{D_0} = 1 - \frac{d_1}{d_0}, \quad (2)$$

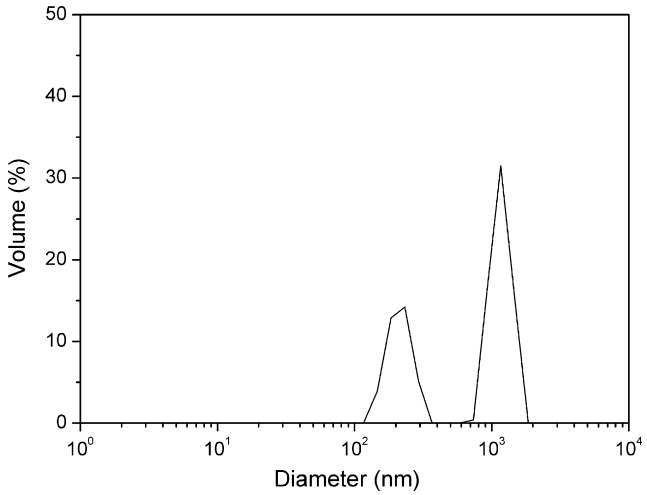

Fig. 2. Particle distribution of the YSZ-8 powder calcined at 900 °C after manual grinding.

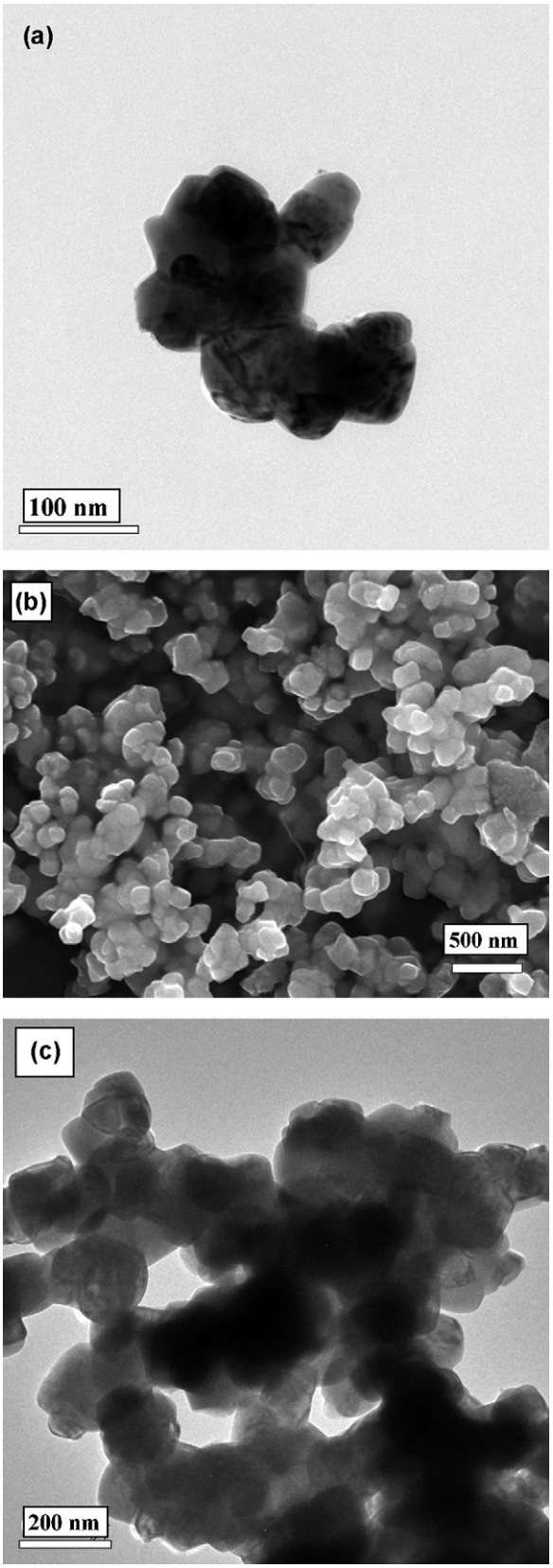

Fig. 3. TEM (a, c) and SEM (b) images of the YSZ-8 powder calcined at 900 °C after manual grinding.

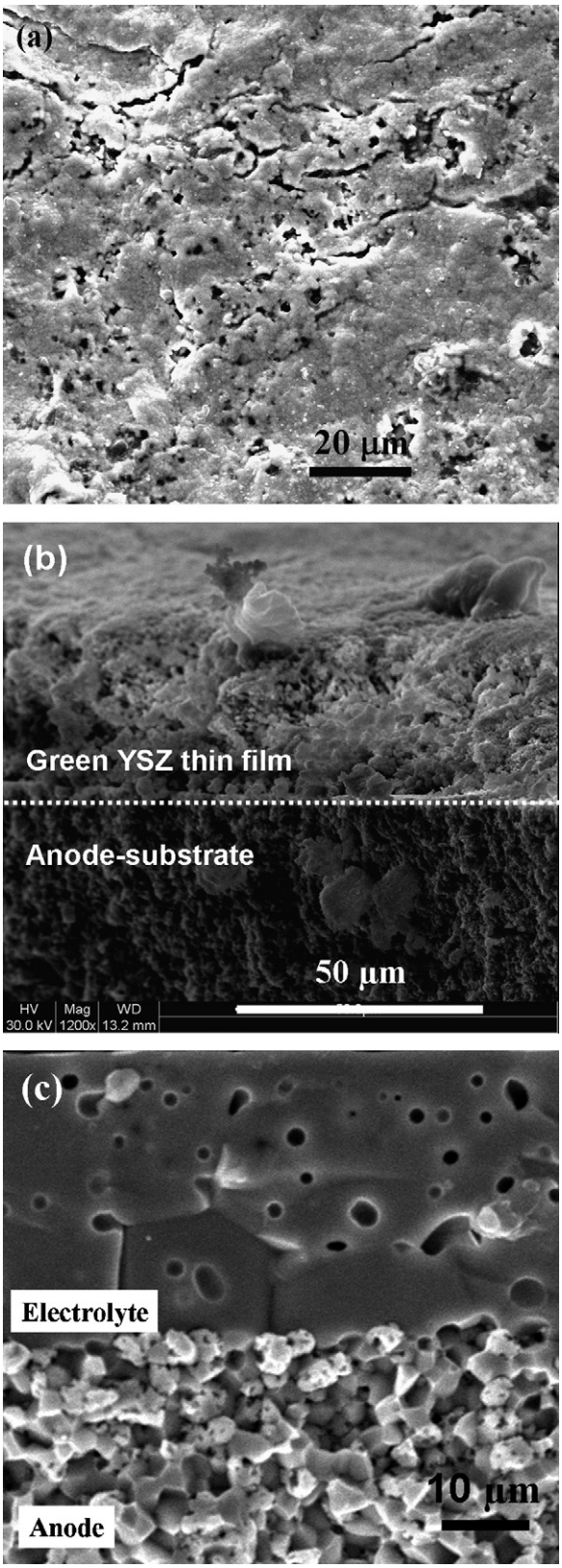

Fig. 4. SEM images of the surface (a) and cross-sections (b, c) of the electrolyte fabricated by WPS using manual grinding YSZ-8 suspension: (b) before sintering and (a, c) after sintering.

or

$$S_A = 1 - \frac{\sqrt[3]{(\pi D_1^2 d_1)/4}}{\sqrt[3]{(\pi D_0^2 d_0)/4}} = 1 - \frac{\sqrt[3]{V_1}}{\sqrt[3]{V_0}} = 1 - \frac{\sqrt[3]{m/\rho_1}}{\sqrt[3]{m/\rho_0}} = 1 - \frac{\sqrt[3]{\rho_0}}{\sqrt[3]{\rho_1}}, \quad (3)$$

where D_0 and d_0 are the diameter and the thickness of the green YSZ-8 thin film, and D_1 and d_1 are the diameter and the thickness of the sintered YSZ-8 thin film, respectively; V_0 and ρ_0 are the volume and the packing density of the green YSZ-8 thin film, and V_1 and ρ_1 are the volume and the density of the sintered YSZ-8 thin film, respectively. This equation indicates that the required shrinkage of the anode-substrate is determined by the packing density of the green YSZ-8 thin film. The higher the packing density of the green thin film, the less shrinkage of the anode-substrate is needed to achieve a fully densified thin electrolyte film.

As shown in Figs. 2 and 3, there was still serious agglomeration in the powder prepared by the EDTA–citrate complexing process even after manual grinding. Such agglomerates resulted in a low green density of the powder due to the presence of many pores and voids inside the agglomerates. A green density of as small as 3% has been reported for the powder prepared by the EDTA–citrate complexing process [29]. Such a low green density is actually beneficial for the fabrication of a thin electrolyte film on a substrate by a co-pressing technique [29,30]. Since the mechanical press can break the soft agglomerates easily, a high packing density of ~60% can be achieved for the green electrolyte layer prepared by the co-pressing technique. As to the green YSZ-8 thin film prepared by the WPS process, the particles were packed under the drive of liquid vehicles (EG). The relatively weak driving force of the liquid vehicle inputted on the powder could not break up the agglomerates during the spraying process. Such loosely packed agglomerates resulted in a low packing density of the green YSZ-8 thin film. The green density of the powder that had been subjected to manual grinding, reached only ~0.96 g cm^{-3} with a relative density of ~16.7%, in comparison to ~4.5% for the freshly synthesized YSZ-8 powder. Assuming the identical shrinkage for the thin film in three dimensions during sintering, the shrinkage of the anode-substrate should reach as large as 44.9% in order to achieve a relative density of 100% for a gas-tight dense electrolyte. However, the sintering shrinkage of the current anode-substrate reached only ~15.7%. Although the *z*-direction perpendicular to the membrane surface is free of constraint during the sintering and may shrink more significantly than the *x*, *y* directions, such a large difference between the shrinkage of the anode and the required shrinkage of the thin-film layer implies that the YSZ-8 thin film is under a large tension during the sintering, which likely causes the formation of large cracks in the electrolyte during the sintering.

The cross-sectional morphologies of the green and sintered YSZ-8 thin films are shown in Fig. 4b and c. There are considerable voids with a size of about 2–5 μm observed for the green YSZ-8 thin film. After the sintering, there are many enclosed pores including cracks formed in the bulk of the electrolyte. Such pores are detrimental to the ionic conduction in the electrolyte by blocking the oxygen diffusion paths. Kingery and Francois [31] suggested that, for a given packing form, whether a pore shrinks or not during sintering is dependent on the pore coordination number *P*. If $P < P_C$ (critical pore coordination number, denoted P_C), the surface of the pore will move toward its center of curvature and the decrease in the pore surface energy is greater than the increase in the grain-boundary energy, so the pore will shrink. On the contrary, if $P > P_C$, the pore will grow. For the manually ground YSZ-8 suspension, the agglomerates have a large number of voids, which led to not only the low packing density but also to a high pore coordination number. The formation of the enclosed holes and cracks is then closely related to the agglomerates inside the green layer. The mechanism for the

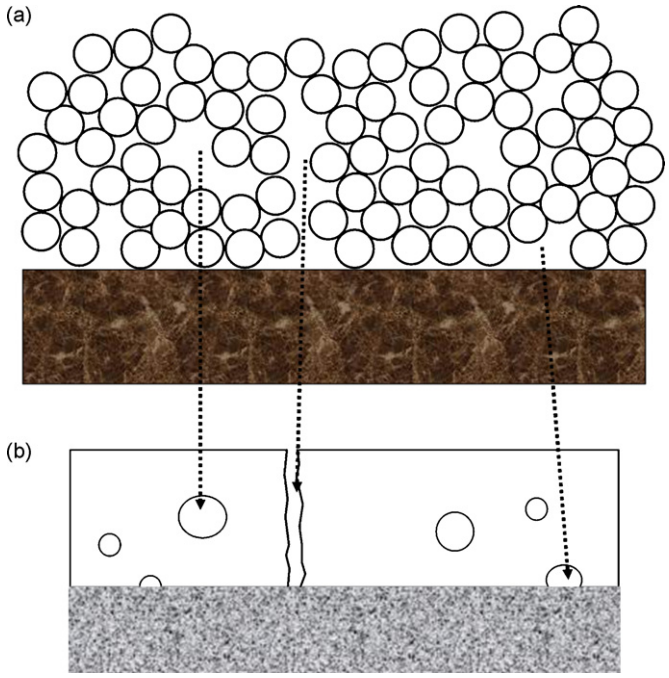

Fig. 5. Schematic of the enclosed hole-forming mechanism for the electrolyte fabricated by WPS using manual grinding YSZ-8 suspension. (a) Before sintering and (b) after sintering.

formation of such holes and cracks is schematically shown in Fig. 5. Improving the packing density of the green YSZ thin film is critical to obtain a crack-free dense thin electrolyte film by WPS process.

It was reported that the agglomerates can be effectively broken by mechanical milling [32,33]. In order to improve the packing density of the thin electrolyte film by WPS with the electrolyte powder prepared from the EDTA–citrate complexing process, the powder was then subjected to high-energy ball milling before deposition. Fig. 6 shows the particle size distribution of the YSZ-8 suspension after high-energy ball milling at 500 rpm for 30 min. Only one sharp distribution peak was observed with a main particle size of ~220 nm, while the distribution peak at around 1 μm that was in the manually ground samples had totally disappeared after the ball milling. It implies that the agglomerates in the original powder were successfully broken up after the high-energy ball milling. The

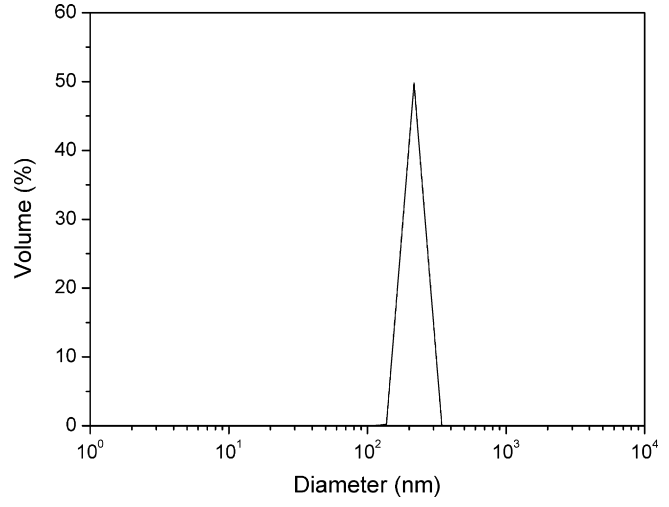

Fig. 6. Particle distribution of the YSZ-8 powder after high-energy ball milling.

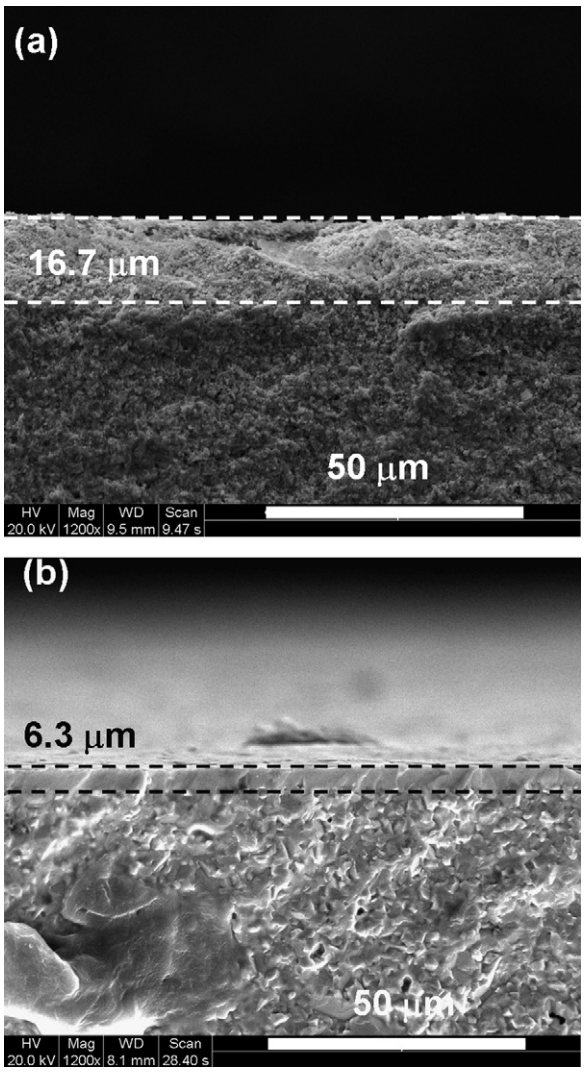

Fig. 7. SEM images of the anode-supported green (a) and densified (b) YSZ-8 thin film.

green density of the high-energy ball milled YSZ-8 powder now reached 1.92 g cm^{-3}, amounting to a relative density of ~32.2%. To obtain a relative density of 100% for the sintered YSZ-8 thin film, the shrinkage of the anode-substrate should reach 30.7% assuming the uniform constriction in all three dimensions. The packing density of the YSZ-8 thin film was also estimated from the volume change of the thin film after sintering. A 1000 °C pre-calcined anode-substrate was used as the substrate. The thicknesses of the thin film are 16.7 and 6.3 μm (measured by SEM shown in Fig. 7), and the diameters of the thin film are 14.6 and 12.5 mm (measured with a vernier caliper), before and after sintering, respectively. By assuming the density of the sintered electrolyte is 100% after sintering, the packing density of the thin electrolyte film reaches ~27.7%, which is slightly smaller than the green density of the starting powder. This suggests that the organics in the suspension may result in looser packing of the YSZ-8 powders in the green thin film. The shrinkage of the electrolyte in the unconstrained *z*-direction is as high as 62.3%, which is much higher than that in *x*, *y* directions (14.3%). Such a large shrinkage in the *z*-direction is beneficial because the required shrinkage of the anode-substrate is lowered significantly.

The typical SEM morphologies of the green dual-layer cell and the sintered one prepared using a ball-milled YSZ-8 powder are shown in Fig. 8. Compared to the one prepared from the manu-

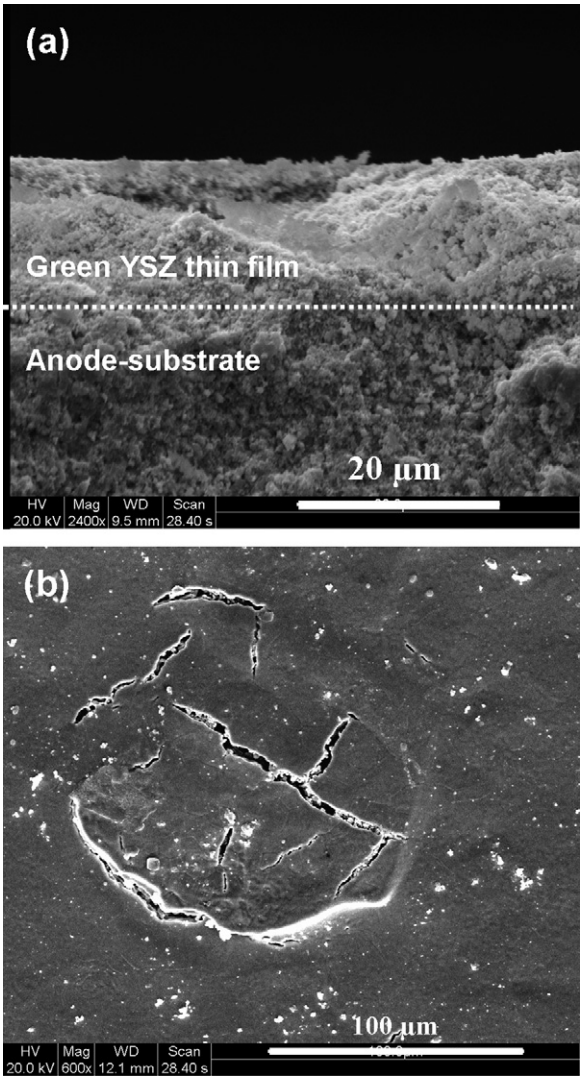

Fig. 8. The typical SEM morphologies of the green dual-layer cell (a), and the sintered one (b) prepared using the high-energy ball-milled YSZ-8 powder.

ally ground YSZ-8 powder, the green thin film prepared from the ball-milled powder is obviously more compact with no observable large voids. After the high-temperature sintering, most part of the thin film was well densified and had adhered to the anode substrate fairly well. However, in some areas, serious cracks are still observed with a length of ~100 μm. In order to obtain a defect-free anode-substrate, some organic additives were introduced into the anode powder purposefully, as described in Section 2. The organics in the anode-substrate, however, were oxidized to CO_2 and H_2O during the sintering. During the oxidation, it produced ~110 mL of gases (standard temperature pressure, and STP) per gram of green anode-substrate. Once there were not enough channels for the gas to vent, the gas could be trapped inside the anode. With increasing the temperature, the gas pressure increased steadily. After the pressure reached a critical value, the tension became so great that it finally cracked the electrolyte layer to release the pressure. The mechanism for the crack-formation over the YSZ-8 thin film deposited on organics-containing anode is schematically shown in Fig. 9.

In order to avoid the detrimental effect of gas formation on the quality of the YSZ-8 thin film, a pre-calcination of the anode-substrate was adopted to eliminate the organics in the substrate before the thin-film layer deposition. However, the pre-calcination

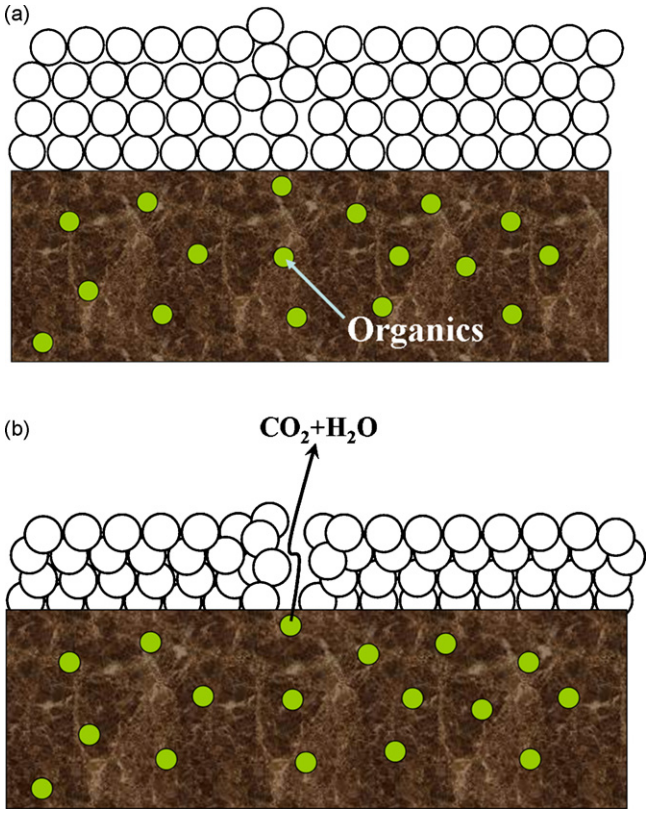

Fig. 9. Schematic of crack-forming mechanism for the electrolyte fabricated on the substrate without pre-calcination: (a) before sintering and (b) during sintering.

would result in a decrease of anode shrinkage and a deterioration of the mechanical strength of the anode-substrate. Therefore, the heating of the anode-substrate should be controlled elaborately. Fig. 10 shows the effect of pre-calcination temperature on the second shrinkage of the anode-substrate. The second shrinkage reached only 13.7% and 14.8%, respectively, when the pre-calcination temperatures were 1100 and 1000 °C. On the other hand, the anode-substrate had very poor mechanical strength when it was pre-calcined at 900 °C due to the weak adhesion between particles. As previously demonstrated, the anode-substrate shrank

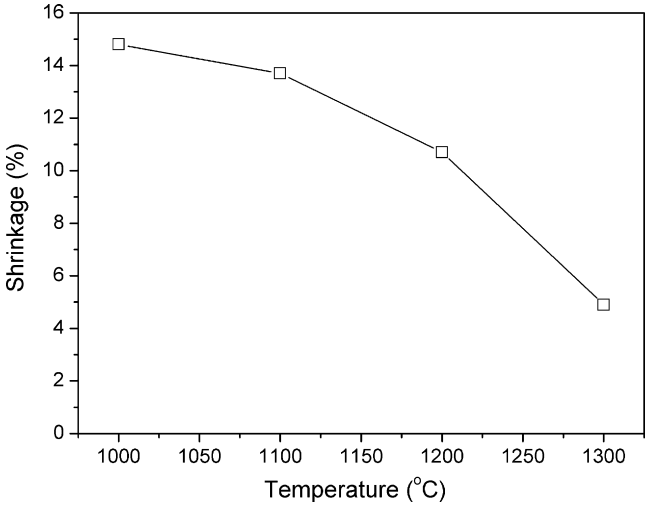

Fig. 10. Effect of the pre-calcination temperature on the second shrinkage of anode-substrate.

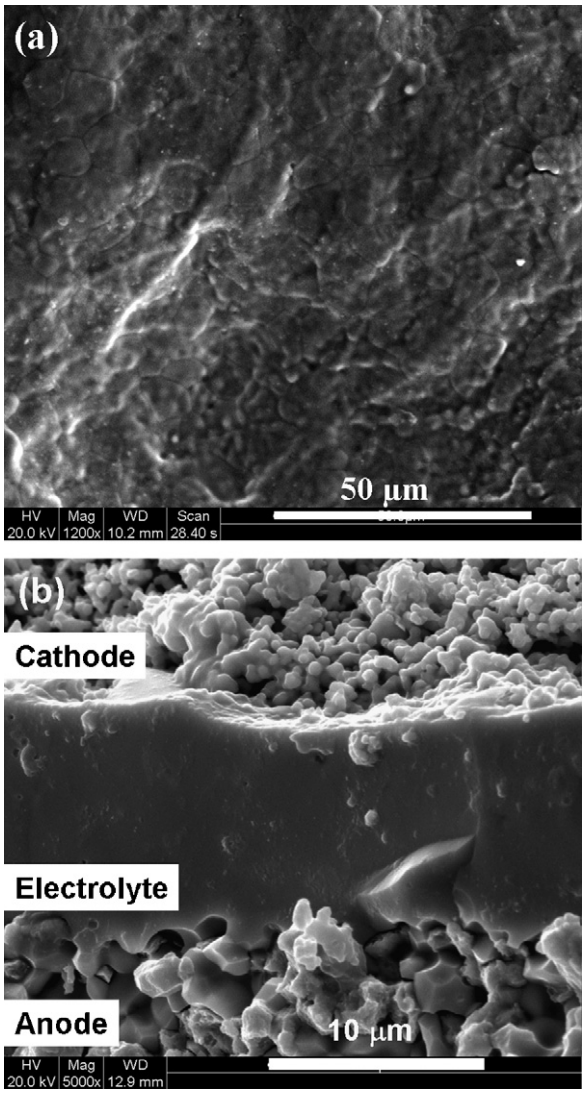

Fig. 11. SEM images of the surface (a), and cross-section (b) of the YSZ-8 electrolyte fabricated on the pre-calcined substrate.

about 14.6% after sintering for the dual-layer green cells; the second shrinkage of the anode-substrate is nearest to this shrinkage after it was pre-calcined at 1000 °C. Therefore, the anode-substrate was subjected to pre-calcination at 1000 °C before thin-film layer deposition. Fig. 11 shows the surface and the cross-sectional morphologies of the electrolyte after sintering at 1400 °C for 5 h by adopting the 1000 °C pre-calcined anode as the substrate. The electrolyte layer was well densified, and it adhered to the anode-substrate fairly well. By examination of the whole electrolyte surface by SEM, no crack was observable. It suggests that a pre-calcination of the anode-substrate at the proper temperature is critical to obtain a crack-free dense thin electrolyte film.

Single cells were then constructed from the dual-layer cells by applying LSM perovskite as the cathode. The fuel cell performance was then examined by *I–V* characterization. Fig. 12 shows the measured OCVs of the fabricated cell as a function of temperature with air as cathode atmosphere and hydrogen as the anode fuel. For comparison, the theoretical values are also presented. The OCV is closely related to the densification of the electrolyte as well as the operating conditions. Cracks and penetrated pinholes in the electrolyte layer would result in mixed potentials over the anode and cathode, and lead to substantially lower OCVs than the theoretical values.

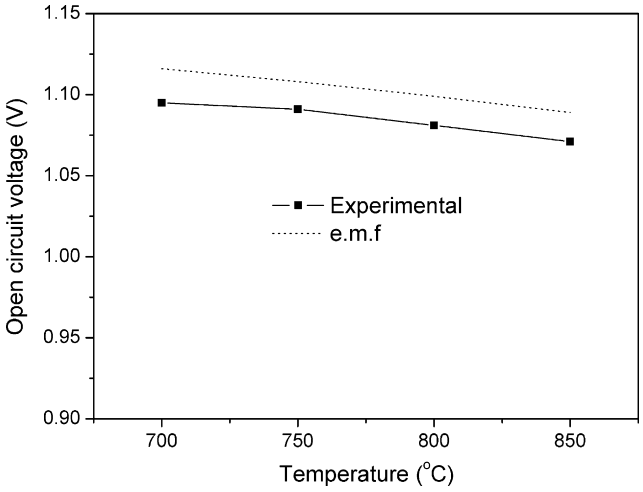

Fig. 12. OCVs of a single cell as a function of temperature.

The observed OCVs are close to the theoretical values, suggesting that the thin electrolyte film is well densified, agreeing well with the SEM observations. The slight difference between the e.m.f. and the OCVs of the single cell may come from the hydrogen permeating the sealant, which may yield the mixed potential resulting from the following reactions:

$$H_2 \rightarrow 2H^+ + 2e^- \quad (4)$$

$$\tfrac{1}{2}O_2 + 2H^+ + 2e^- \rightarrow H_2O \quad (5)$$

Some studies indicated that this H_2 loss should be responsible for the disagreement between the OCVs and e.m.f. values [34–37].

Fig. 13 shows the cell voltages and power densities for a single cell with a 20 μm thick YSZ-8 thin film sintered at 1400 °C. The peak power densities of the single cell are 206, 276, 401, and 567 mW cm^{-2} at 700, 750, 800, and 850 °C, respectively. Fig. 14 further shows the cell voltages and power densities for a single cell tested at 850 °C as a function of electrolytic thickness. The peak power densities are 894, 567, and 307 mW cm^{-2} and the OCVs are 1.068, 1.071, and 1.092 V for the single cells with the electrolytic thicknesses of 10, 20, and 50 μm, respectively. The corresponding EIS measured under the OCV conditions are shown in Fig. 15. Here, the intercept with the real axis at high frequencies represents the ohmic resistance of the electrolyte and lead wires. As expected, the ohmic resistances increase steadily with increasing the electrolytic

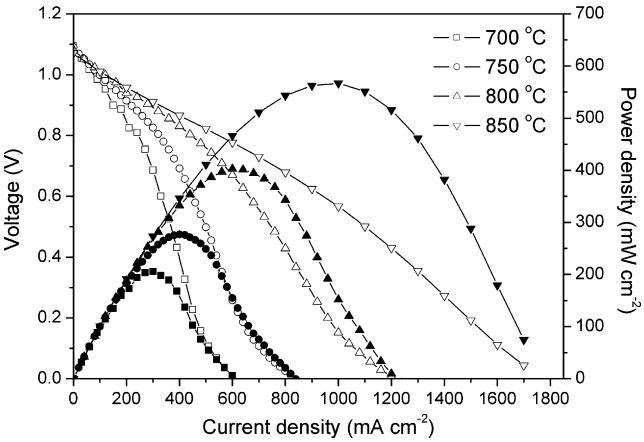

Fig. 13. *I–V*, *I–W* curves of a single cell with a 10-μm thick YSZ-8 electrolyte as a function of temperature.

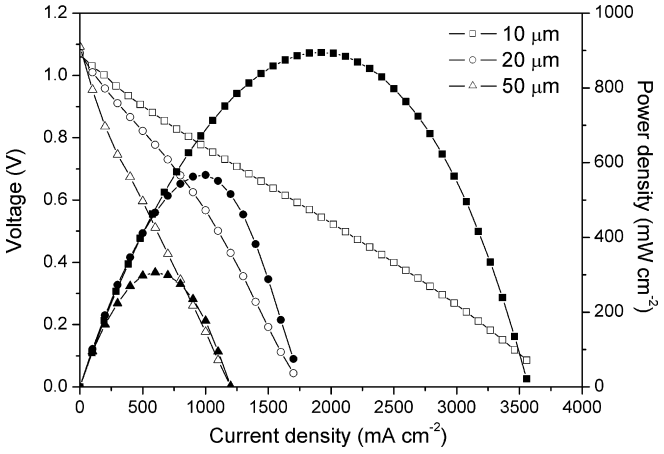

Fig. 14. *I–V*, *I–W* curves of the single cells with various electrolytic thicknesses operated at 850 °C.

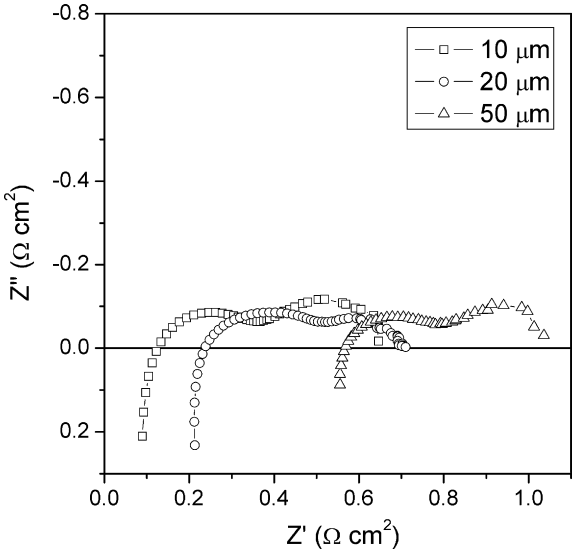

Fig. 15. Impedance spectra for the single cells with various electrolytic thicknesses operated at 850 °C.

thicknesses, i.e. 0.127, 0.239, and 0.564 Ω cm^2 for the single cells with the electrolytic thicknesses of 10, 20, and 50 μm, respectively. The resistance between the two intercepts with the real axis corresponds to the impedance of the two interfaces, i.e. the cathode–electrolyte interface and the anode–electrolyte interface. Since the anodes and cathodes are nominally identical, the area specific resistances of electrodes are very similar. It should be noted that the power density is not in reverse proportion to the electrolytic thickness. For example, the peak power density of the cell with a 10-μm thick electrolyte is only about three times that of the cell with a 50-μm thick electrolyte. It suggests that the resistance from the electrodes plays a significant role in the fuel cell performance in this study. This is reasonable because LSM is not a good performance cathode at intermediate temperatures. It is expected that even higher power densities can be achieved by optimizing the electrode composition.

4. Conclusions

A WPS process is successfully applied to fabricate a dense YSZ-8 thin film on an anode-substrate for a solid-oxide fuel cell application. Agglomerates in as-prepared YSZ-8 powders result in a low packing density of YSZ-8 green thin film, and which induce the formation of cracks and enclosed holes inside the thin electrolyte film during the sintering. High-energy ball milling is an efficient method to break up such agglomerates and substantially increases the packing density of the green thin film. On the other hand, the anode-substrate also has a significant influence on the sintering process of the electrolyte. Gases that are produced from the pyrolysis of organics in the anode added during the substrate fabrication would break the electrolyte during the sintering. Pre-calcination of the substrate at ~1000 °C can effectively eliminate its effect on the quality of the thin film, also the second shrinkage of the anode matches well with the YSZ-8 thin film. Accordingly, the crack-free dense YSZ-8 thin film was fabricated with a thickness as low as 10 μm. The corresponding open circuit voltage of the single cell based on a $La_{0.8}Sr_{0.2}MnO_3$ cathode is 1.071 V, and the peak power density is as high as 894 mW cm^{-2} at 850 °C.

Acknowledgements

This work was supported by the National Natural Science Foundation of China under Contract Nos. 20646002 and 20676061, by the National 863 program under Contract No. 2007AA05Z133, and by the National Basic Research Program of China under Contract No. 2007CB209704.

References

[1] R. Doshi, V.L. Richards, J.D. Carter, X.P. Wang, M. Krumpelt, J. Electrochem. Soc. 146 (1999) 1273–1278.
[2] M.G. Bellino, D.G. Lamas, N.E. Walsöe de Reca, Adv. Funct. Mater. 16 (2006) 107–113.
[3] A. Infortuna, A.S. Harvey, L.J. Gauckler, Adv. Funct. Mater. 18 (2008) 127–135.
[4] J.H. Shim, C.-C. Chao, H. Huang, F.B. Prinz, Chem. Mater. 19 (2007) 3850–3854.
[5] J. Will, A. Mitterdorfer, C. Kleinlogel, D. Perednis, L.J. Gauckler, Solid State Ionics 131 (2000) 79–96.
[6] H. Yamane, T. Hirai, J. Mater. Sci. Lett. 6 (1987) 1229–1230.
[7] U. Pal, S.C. Singhal, J. Electrochem. Soc. 137 (1990) 2937–2941.
[8] L.W. Tai, P.A. Lessing, J. Am. Ceram. Soc. 74 (1991) 501–504.
[9] W.J. Daughton, S.L. Givens, J. Electrochem. Soc. 129 (1982) 173–179.
[10] K. Mehta, R. Xu, Y.V. Virkar, J. Sol–Gel Sci. Technol. 11 (1998) 203–207.
[11] W.T. Bao, W. Zhu, G.Y. Zhu, J.F. Gao, G.Y. Meng, Solid State Ionics 176 (2005) 669–674.
[12] J. Liu, S.A. Barnett, J. Am. Ceram. Soc. 85 (2002) 3096–3098.
[13] Z. Cai, T.N. Lan, S. Wang, M. Dokiya, Solid State Ionics 152–153 (2002) 583–590.
[14] W.T. Bao, Q.B. Chang, R.Q. Yan, G.Y. Meng, J. Membr. Sci. 252 (2005) 175–181.
[15] J.-H. Song, S.-I. Park, J.-H. Lee, H.-S. Kim, J. Mater. Process. Technol. 198 (2008) 414–418.
[16] H. Moon, S.D. Kim, S.H. Hyun, H.S. Kim, Int. J. Hydrogen Energy 33 (2008) 1758–1768.
[17] R. Hui, Z.W. Wang, S. Yick, R. Maric, D. Ghosh, J. Power Sources 172 (2007) 840–844.
[18] G. Dell'Agli, S. Esposito, G. Mascolo, M.C. Mascolo, C. Pagliuca, J. Eur. Ceram. Soc. 25 (2005) 2017–2021.
[19] X.D. Ge, X.Q. Huang, Y.H. Zhang, Z. Lu, J.H. Xu, K.F. Chen, D.W. Dong, Z.G. Liu, J.P. Miao, W.H. Su, J. Power Sources 159 (2006) 1048–1050.
[20] R.R. Peng, C.R. Xia, X.Q. Liu, D.K. Peng, G.Y. Meng, Solid State Ionics 152–153 (2002) 561–565.
[21] K. Wippermann, U. Stimming, H. Jansen, D. Stover, in: S.C. Singhal, H. Iwahara (Eds.), Electrochemical Behavior of Perovskite Cathodes Made by Wet Powder Spraying, SOFC III, The Electrochemical Society, Pennington, NJ, 1993, pp. 180–189, PV 93–94.
[22] N.M. Sammes, M.S. Brown, R. Ratnaraj, J. Mater. Sci. Lett. 13 (1994) 1124–1126.
[23] V. Dusastre, J.A. Kilner, Solid State Ionics 126 (1999) 163–174.
[24] N. Oishi, Y. Yoo, I. Davidson, J. Am. Ceram. Soc. 90 (2007) 1365–1369.
[25] E. Schüller, R. Vaßen, D. Stöver, Adv. Eng. Mater. 4 (2002) 659–662.
[26] K. Xie, R.Q. Yan, D.H. Dong, S.L. Wang, X.R. Chen, T. Jiang, B. Lin, M. Wei, X.Q. Liu, G.Y. Meng, J. Power Sources 179 (2008) 576–583.
[27] K. Xie, Q.L. Ma, B. Lin, Y.Z. Jiang, J.F. Gao, X.Q. Liu, G.Y. Meng, J. Power Sources 170 (2007) 38–41.
[28] W. Zhou, Z.P. Shao, W.Q. Jin, J. Alloys Compd. 426 (2006) 368–374.
[29] H.X. Gu, R. Ran, W. Zhou, Z.P. Shao, J. Power Sources 172 (2007) 704–712.
[30] C.R. Xia, M.L. Liu, J. Am. Ceram. Soc. 84 (2001) 1903–1905.
[31] W.D. Kingery, B. Francois, in: G.C. Kuczynski, N.A. Hooton, G.F. Gibbon (Eds.), Sintering and Related Phenomena, Gordon Breach, NY, 1967, p. 471.

[32] S. Coste, G. Bertrand, C. Coddet, E. Gaffet, H. Hahn, H. Sieger, J. Alloys Compd. 434–435 (2007) 489–492.
[33] T.S. Zhang, J. Ma, L.B. Kong, P. Hing, Y.J. Leng, S.H. Chan, J.A. Kilner, J. Power Sources 124 (2003) 26–33.
[34] N. Miura, G. Lu, N. Yamazoe, Solid State Ionics 136–137 (2000) 533–542.
[35] A. Tomita, Y. Namekata, M. Nagao, T. Hibino, J. Electrochem. Soc. 154 (2007) J172–J176.
[36] T. Hibino, A. Hashimoto, S. Kakimoto, M. Sano, J. Electrochem. Soc. 148 (2001) H1–H5.
[37] T. Hibino, S. Tanimoto, S. Kakimoto, M. Sano, Electrochem. Solid-State Lett. 2 (1999) 651–653.